JCTC Journal of Chemical Theory and Computation

Article

pubs.acs.org/JCTC

Benchmarking Time-Dependent Density Functional Theory for Excited State Geometries of Organic Molecules in Gas-Phase and in Solution

Ciro A. Guido,*[,†] Stefan Knecht,*[,‡] Jacob Kongsted,*[,‡] and Benedetta Mennucci*[,¶]

[†]Laboratoire Structures, Propriétés et Modélisation des Solides (SPMS), CNRS UMR 8580, École Centrale Paris, Grande Voie des Vignes, F-92295 Châtenay-Malabry, France

[‡]Department of Physics, Chemistry and Pharmacy, University of Southern Denmark, Campusvej 55, 5230 Odense M, Denmark

[¶]Dipartimento di Chimica e Chimica Industriale, Università di Pisa, via Risorgimento 35, I-56126 Pisa, Italy

ABSTRACT: We analyze potentials and limits of the Time-Dependent Density Functional Theory (TD-DFT) approach for the determination of excited-state geometries of organic molecules in gas-phase and in solution. Three very popular DFT exchange-correlation functionals, two hybrids (B3LYP and PBE0) and one long-range corrected (CAM-B3LYP), are here investigated, and the results are compared to the correlated RI-CC2 wave function approach. Solvent effects are further analyzed by means of a polarizable continuum model. A total of 15 organic chromophores (including both small molecules and larger push−pull systems) are considered as prototypes of $n \rightarrow \pi^*$ and $\pi \rightarrow \pi^*$ singlet excitations. Our analysis allows to point out specific correlations between the accuracy of the various functionals and the type of excitation and/or the type of chemical bonds involved. We find that while the best ground-state geometries are obtained with PBE0 and B3LYP, CAM-B3LYP yields the most accurate description of electronic and geometrical characteristics of excited states, both in gas-phase and in solution.

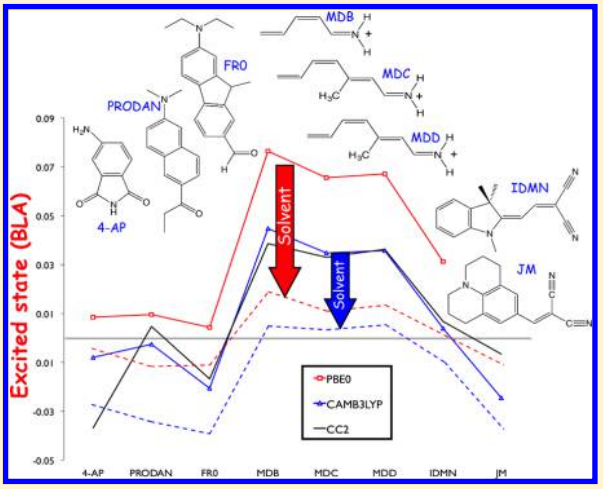

1. INTRODUCTION

Extension of Density Functional Theory (DFT) to electronically excited states, namely, Time-Dependent Density Functional Theory (TD-DFT), was proposed more than 25 years ago[1,2] and in the years since then it has become the most popular approach for the computation of transition energies as well as for the evaluation of excited state structures and properties. This enormous success, however, cannot hide the important limitations that TD-DFT has in its present formulations. First of all, because it relies on a single determinant description of the ground state wave function, TD-DFT is inadequate when multiple states are energetically close or when the excited state cannot be described in terms of single excitations. Moreover, the reliability of the results depends significantly on the selected exchange-correlation (xc) functional and finally, TD-DFT presents a specific drawback for certain kinds of excitations, for example, those largely characterized by a charge-transfer.[3] This drawback originates from the inability of the actual implementations of TD-DFT to follow the reorganization of charge between two separated regions of space or between orbitals of different spatial extent.

This brief summary of the major drawbacks of TD-DFT clearly emphasizes the importance of extended and articulate benchmark studies. In fact, only a detailed knowledge of the limits and the potentials of the various functionals for the different types of excitations and molecular systems can prevent incorrect applications of the method. In the literature many benchmark studies of this type are available; however, most of these are limited to vertical transition energies[4−13] and related transition properties while much less is known about excited state geometries,[14−17] even if an analysis on the TD-DFT performances in determining excited state structures of organic molecules with respect to CASPT2 was performed by some of the present authors (C.A.G. and B.M.).[18] However, no extensive studies have so far been presented to detail how different DFT functionals can describe excitation and excited state structures of solvated systems. This is indeed an important aspect since the electronic processes of interest are generally in solution or in more complex environments such as protein matrixes, interfaces and membranes, composite liquid−solid systems, and so forth. Nowadays, many studies are available in

Received: January 10, 2013
Published: March 18, 2013

ACS Publications © 2013 American Chemical Society

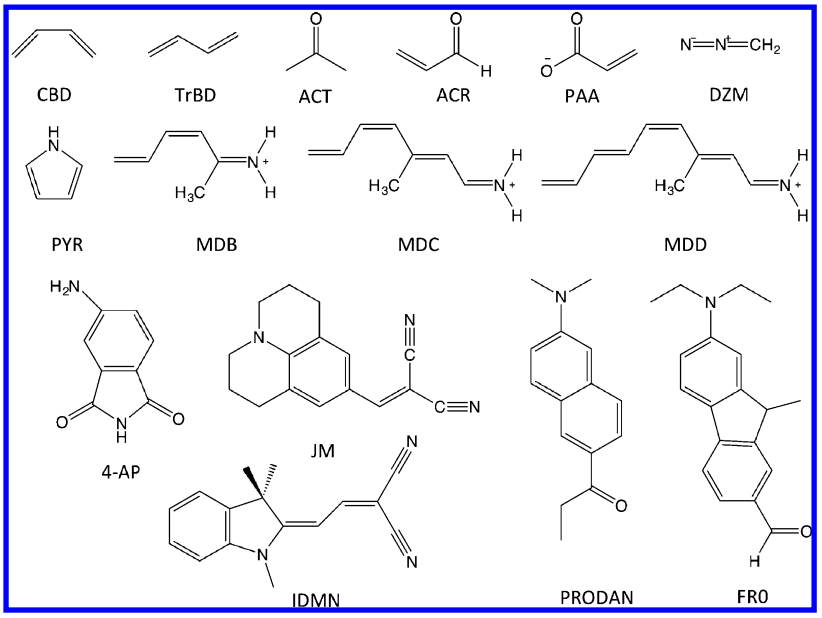

Figure 1. Reference set of molecules used in this study. From left to right and top to bottom: *cis*-buta-1,3-diene (CBD); *trans*-buta-1,3-diene (TrBD); acetone (ACT); acrolein (ACR); propenoic acid anion (PAA); diazomethane (DZM); pyrrole (PYR); three model systems of a protonated Schiff's base (MDB, MDC, and MDD); 4-aminophtalimide (4-AP); julolidine-malononitrile (JM); indolinedimethine-malononitrile (IDMN); 6-propionyl-2-dimethylamino naphtalene (PRODAN); 7-diethylamino-9.9-dimethyl-9*H*-fluorene-2-carbaldehyde (FR0).

the literature in which the TD-DFT approach is combined with different solvation models with the aim to provide insights on both the absorption and the fluorescence properties of solvated or embedded chromophores (for an exhaustive list of references on this subject see refs 16,19,20). However, in most of these studies only minor attention, or none at all, is paid to the possibility that a well-suited functional for isolated systems could perform less accurate in solution because the good results obtained in gas-phase are a result of a cancellation of errors which is no longer valid when solvent effects are included in the calculation. A related issue is that different exchange-correlation functionals may lead to different degrees of charge separation in either ground or excited states and because of this a different (increased/decreased) interaction between the solute and the solvent may be observed. Thus even if functionals perform reasonably similarly in vacuum, even small differences in the predicted charge distributions may be amplified when the system is placed in an environment.

Recently, simulations of the adiabatic energies of 40 fluorescent molecules in solution[21] were performed combining different hybrid functionals with the polarizable continuum model (PCM)[22] to include solvent effects. Overall, the functionals providing the smallest mean absolute error were PBE0[23,24] and M06[25] but at the price of a rather limited consistency (R = 0.89), which was explained by qualitatively incorrect excited-state geometries obtained for specific molecules using PBE0 (and other similar hybrids). Both M06-2X and CAM-B3LYP[26] instead avoided these qualitative failures and allowed one to improve the experiment/theory correlation (R = 0.95) without significantly deteriorating the mean deviation (MAE of 0.25 eV). In the present study we continue along the same line but we here specifically focus on the geometrical parameters and we compare three of the previously investigated functionals (B3LYP,[27,28] PBE0, CAM-B3LYP) combined with PCM for the determination of the geometry relaxation upon excitation for solvated systems.

In this analysis we have selected 15 molecules to obtain a representative set of typical organic chromophores. To define this selection we started by extracting a subset of molecules from the benchmark set proposed by Schreiber et al.,[29] and we augmented this set with larger molecules from earlier benchmark calculations performed by some of us (C.A.G. and B.M.).[18,30,31] To cover the large variety of chemical motifs present in typical organic chromophores, the selected reference set of organic molecules ranges from unsaturated aliphatic hydrocarbons, aldehydes, and ketones to aromatic hydrocarbons and heterocycles. Acronyms for each molecule are given in Figure 1. For the sake of brevity we will make use of these acronyms throughout this paper.

The present selection of molecules allows us to analyze both $n \rightarrow \pi^*$ (PAA, DZM, ACR, ACT) and $\pi \rightarrow \pi^*$ (CBD, TrBD, PYR, MDB, MDC, MDD, 4-AP, JM, IDMN, FR0, PRODAN) transitions, as well as to quantify the effects of combining a possible charge-transfer character of the excitation with solvent effects.

The paper is organized in two main parts, one comparing the investigated DFT functionals with the resolution-of-identity (RI) second order Coupled Cluster (CC2)[32,33] approach for gas-phase systems (Section 3.1), and one discussing the DFT results computed in combination with the integral equation formalism (IEF) version of PCM[34] in both polar and apolar solvents in light of the trends found from the gas-phase benchmarks (Section 3.2).

2. COMPUTATIONAL DETAILS

2.1. RI-CC2. All CC2 calculations were performed with the implementation[33,35,36] available in the quantum chemistry program package Turbomole.[37] In the CC2 model the parent CCSD approach is approximated by keeping the singles equations and truncating the doubles equations to first order in the fluctuation potential.[32] Bearing this in mind, quantitatively good results could be expected for single-reference ground states and excited states that are governed

by single excitations. To reduce the computational cost we employed for the CC2 *ansatz* the resolution-of-identity (RI) approximation[33] for the molecular two-electron integrals. Errors made within the RI approximation are, with optimized auxiliary basis sets, in general negligible as compared to errors due to the one-electron basis set incompleteness. We used standard Gaussian basis sets of correlation-consistent triple-ζ quality augmented with diffuse functions (aug−cc-pVTZ, in what follows denoted as aVTZ)[38,39] in combinations with their corresponding optimized auxiliary basis sets.[40] We carried out all geometry optimizations in the highest possible point-group symmetry that could be imposed thereby taking advantage of the available implementations of analytic ground- and excited state gradients[36,41] of the CC response approach. All electrons were correlated in both the ground- and excited state geometry optimizations, and we kept this computational level for the single-point excited state calculations at the respective equilibrium geometries. Additional CC2 response property calculations were performed to determine the oscillator strengths for individual transitions. We furthermore computed in particular cases (*vide infra*) the D_1 and D_2 diagnostics[42,43] for the CC2 ground state wave function together with a measure of the single excitation character[41] which can support an unambiguous identification of shortcomings in the applied CC2 model.

2.2. DFT. All DFT and TD-DFT calculations have been performed using the G09 program package[44] employing three different exchange-correlation (xc) functionals each characterized by having a different amount of exact HF exchange included. The functionals used are (i) B3LYP (20% HF exchange), (ii) PBE0 (25% HF exchange), and (iii) CAM-B3LYP. The latter xc-functional belongs to the class of range-separated hybrid functionals and the amount of HF exchange varies here smoothly between 19% (short-range) and 65% (long-range). Calculation of electronic excitation energies and geometries were based on the linear response time-dependent (TD) approach. All DFT and TD-DFT calculations, that is, both ground- and excited-state energies and structures, made use of the Pople 6-311++G(d,p) basis set. Generally, a medium size basis set (valence double or triple-ζ basis) already gives converged results for valence transitions when both polarization and diffuse functions are added. In particular, Pople's 6-311+G(2d,p) basis set provides converged transition energies of the low-lying states for the majority of the investigated dyes.[45−47] Moreover, in the paper of 2010[18] (and its Supporting Information), two of the present authors (C.A.G. and B.M.) tested the convergence by using seven basis sets for the TD-DFT optimizations, comprising Pople's 6-31G(d), 6-311G(d) as well as Dunning's cc-pVDZ, cc-pVTZ, aug-cc-pVDZ, and aug-cc-pVTZ basis sets for all systems with all functionals used in that article. The obtained results underline that, in general, introducing polarization functions or triple-ζ leads to a shortening of bond lengths, with a dispersion of data around 0.2−0.4%, as it can be argued by RSD values reported in the Supporting Information of the 2010 paper.[18] Pyrrole and propenoic acid anion constitute exceptions: in these cases the results are more basis set dependent with a dispersion of data around 1−2% and behaviors of functional performances in passing from 6-31G* to aug-cc-pVTZ are not so regular as in the other systems. We also checked the dependence of the bond length alternation of a subset of the larger chromophores (not included in our precedent study), by comparing 6-311+G(d,p) and aug-cc-pVTZ based results for CAM-B3LYP: The differences are in all cases below 0.01 Å.

2.3. Solvation Model. Solvent effects were described by exploiting the IEFPCM[34] with a cavity made of interlocking spheres centered on the heavy atoms. The UA0 set of sphere radii implemented in the Gaussian code has been adopted in all PCM calculations: this uses the United Atom Topological Model applied on atomic radii of the UFF force field for heavy atoms whereas the hydrogens are enclosed in the sphere of the bonding heavy atom. Only in the cases of PYR, 4-AP, MDB, MDC, and MDD we have used specific spheres centered on the aminic hydrogens with radii equal to 1.2 Å. Ground- and excited-state geometries were obtained in an equilibrium solvation regime, whereas vertical excitation energies were obtained in the nonequilibrium solvation regime (where only the fast component of solvent polarization is taken in equilibrium with the excited state density). For both absorption and emission vertical energies the corrected linear response (cLR) scheme was adopted.[48] Within the cLR framework, a "state specific" correction to the TD-DFT excitation energies is introduced by using a solvent reaction field calculated in terms of the relaxed density of each electronic state.

3. RESULTS AND DISCUSSION

The selected systems can be divided in two different sets: one collecting the smaller molecules (CBD, TrBD, ACT, ACR, PAA, DZM, and PYR) and one considering the larger conjugated systems (4-AP, PRODAN, FR0, JM, IDMN, MDB, MDC, MDD). In the first set of molecules the analysis focuses on all bond lengths while in the second set a single collective geometrical parameter, the bond length alternation (BLA),[49] is analyzed. The BLA is defined as the difference between the average single- and double bond lengths along a conjugation chain (in Figure 2 the single and double bonds

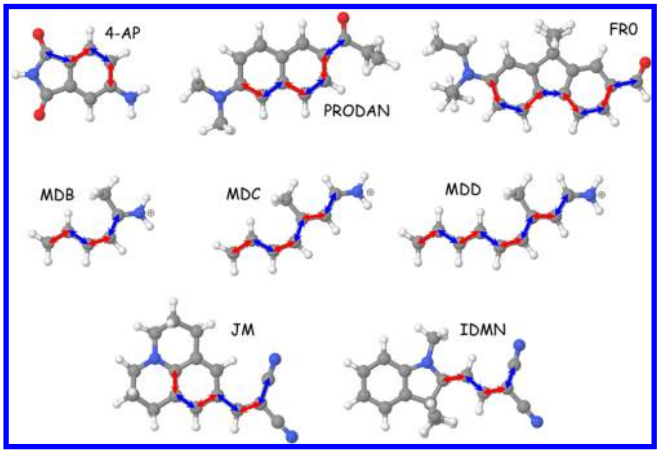

Figure 2. Single (blue) and double (red) bonds included in the definition of the BLA for each of the investigated system.

used to define the BLA for each of the investigated systems are shown). The values of the BLA can be qualitatively correlated to a charge-transfer character of the system. In fact if we introduce a valence-bond like description in terms of the three classical resonance forms (the "neutral", the "cyanine-like", and the "zwitterionic" one), a BLA > 0 can be associated to a system in which the single and double bonds are well localized as shown in Figure 1, a BLA ∼ 0 instead indicates a completely delocalized (i.e., cyanine-like) system, and a BLA < 0 refers to a

dx.doi.org/10.1021/ct400021c | J. Chem. Theory Comput. 2013, 9, 2209−2220

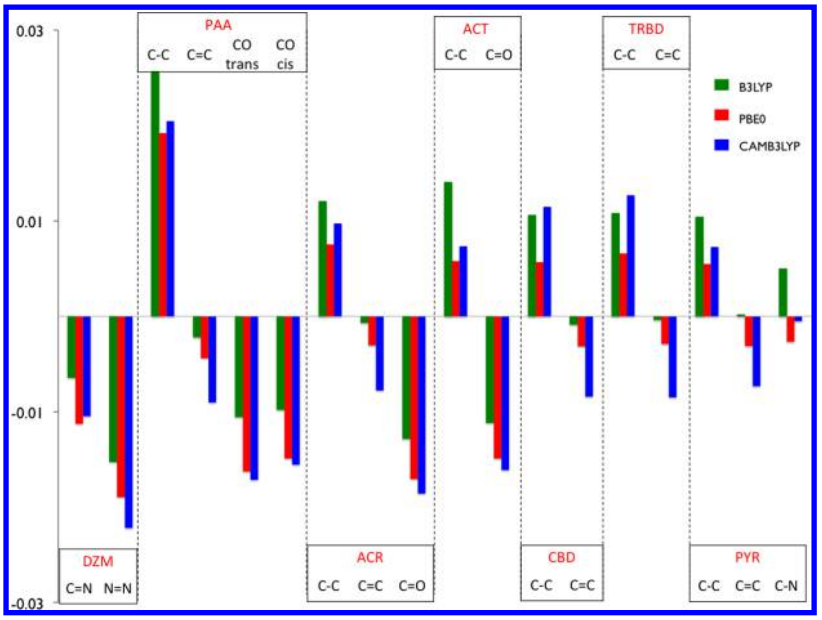

Figure 3. Differences in bond lengths (in Å) of ground state geometries calculated at the DFT/x level with respect to RI-CC2 values.

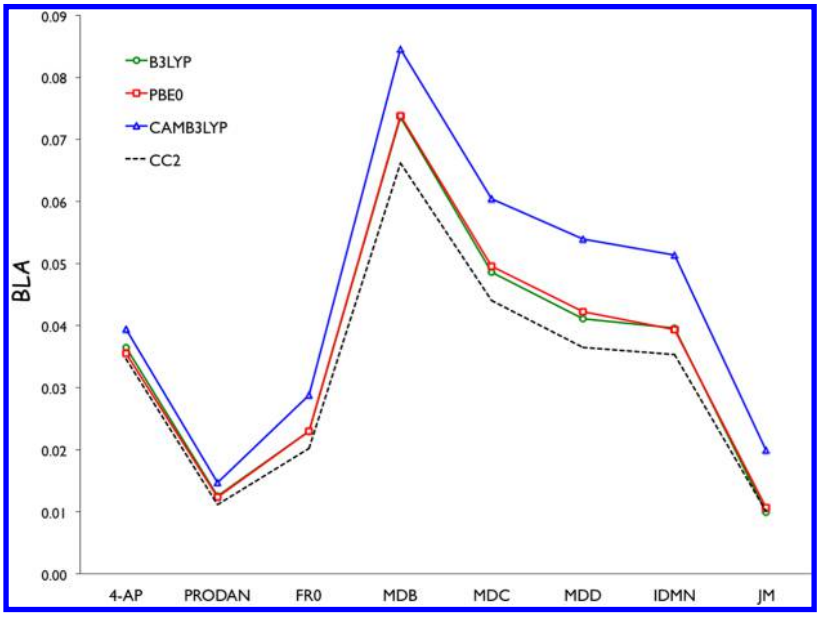

Figure 4. Ground-state bond-length alternation (BLA) computed at the DFT/x and RI-CC2 level of theory. BLA values are in Å.

zwitterionic system where the single and double bonds of the "neutral" structure have been completely reverted.

As discussed in the Introduction, isolated and solvated systems are here analyzed separately. In particular for gas-phase the results obtained using the different DFT functionals are compared to the corresponding ones obtained with RI-CC2 to identify the functional which better describes both ground and excited state structures. Successively for the solvated systems, the solvent-induced shifts obtained with the different functionals are reported and comparatively analyzed.

3.1. Isolated Systems. *3.1.1. Ground State Structures and Absorption Energies.* Since the RI-CC2/aVTZ geometries and excitation energies, respectively, will form our basis for a selection of a suitable functional for further ground- and excited-state studies of organic chromophores we examine first the accuracy of the benchmark data when available.

Page and Olivucci[50] previously optimized ground- and excited state geometries for the six small molecules at the CASSCF and CASPT2 level of theory. RI-CC2/aVTZ consistenty displays a picture of shorter single and double bonds in all ground state molecules with respect to CASPT2 with the exception of the C−C single bond in ACR. Relative deviations are on the order of less than 1% for all bond types, though. Maximum divergences between RI-CC2 and CASPT2 are found for the C−C single bond in PAA and the double bond in CBD, respectively, which are more compact by 0.012 Å and 0.013 Å. Extensive reference studies, however, highlighted that CC2 tends to slightly *overestimate* bond lengths compared to high-level coupled cluster benchmarks in many representative small organic compounds[36,41] where the correlation error stemming from an approximate Coupled Cluster expansion generally surpasses the basis set error already at the aug-cc-pVTZ level.[51] Furthermore, neither of the studied ground state

compounds exhibited noticeable D_1 and D_2 wave function diagnostics. We therefore conclude that the RI-CC2 ground state equilibrium structures are sufficiently accurate for our purposes.

Moving now to DFT ground-state geometries, for all small molecules we find an overall close agreement with the RI-CC2 reference values as illustrated in Figure 3.

Deviations within the DFT approach are generally < ±0.015 Å which also confirms previous conclusions[18] based on a comparison with CASPT2 reference data.[50]

Assessing next the ground state geometries of the larger conjugated systems by virtue of the BLA parameter as displayed in Figure 4, we note that DFT results with either functional are generally in line with their wave function counterparts.

The hybrid functionals PBE0 and B3LYP with a fixed amount of exact Hartree−Fock exchange differ for all systems less than 0.01 Å from the RI-CC2 reference curve. The long-range corrected CAM-B3LYP functional exhibits somewhat larger deviations of up to 0.02 Å and thus overemphasizes the locality of single- and double bonds. RI-CC2, on the other hand, predicts in all cases a most conjugated system. In summary, the shapes of the BLA curves closely match for either approach, particularly the monotonic decrease from MDB, MDC, to MDD, which underlines that the extending spatial charge delocalization with an increasing $\pi-\pi^*$ conjugation chain is captured well by all methods in these model systems.

The analysis of the ground state structures is strictly related to that on the absorption energies which are reported in Table 1 for all the investigated systems in gas-phase: all values have been computed at the corresponding optimized geometries.

Upon inspection of Table 1 a general acceptable agreement between DFT and RI-CC2 data for both excitation classes $n \rightarrow \pi^*$ (PAA, DZM, ACR, ACT) and $\pi \rightarrow \pi^*$ (CBD, TrBD, PYR, MDB, MDC, MDD, 4-AP, JM, IDMN, FR0, PRODAN) is observed with mean absolute error (MAE) around 0.2 eV for all functionals and standard deviation (SD) of 0.12−0.15 eV. Maximum deviations are found for TRBD with B3LYP (−0.52 eV) and PBE0 (−0.41 eV), and for PAA with CAM-B3LYP (+0.45 eV). Furthermore, the oscillator strengths match closely at all levels of theory. Among the three xc-functionals considered here B3LYP consistently provides the lowest excitation energies for all 15 molecules which is in line with previous results using a double-ζ basis set.[18,30] CAM-B3LYP on the contrary tends to exceed RI-CC2 excitation energies on the order of +0.20−0.40 eV, in particular for the $n \rightarrow \pi^*$ transition in PAA as well as the $\pi \rightarrow \pi^*$ transitions in the (hetero)aromatic push−pull type chromophores (JM, IDMN, FR0, PRODAN).

Considering the MDx systems, where the $\pi \rightarrow \pi^*$ excitation energies decrease as expected from MDB → MDD, a similar picture emerges for RI-CC2 with regard to TD-DFT as was observed in ref 18 for CASPT2. Both wave function methods nearly coincide with deviations of less than one-tenth of an eV whereas DFT consistently puts the first singlet excited state at higher energies. The relative downshift in the excitation energies along the MDx series are however predicted correctly within 0.1 eV. Besides, the perfect agreement of the present CC2 transition energies for MDB→MDD with the previous CC2 data of Page and Olivucci[50] (see Table 1), that was computed using a double-ζ basis set, confirms that basis set convergence has indeed been reached for CC2 excitation energies at the level of a triple-ζ basis set.[51]

Table 1. Computed Vertical Absorption Energies (eV) at the DFT/6-311++G(d,p) and RI-CC2/aVTZ Level of Theory[a]

system	B3LYP	PBE0	CAM-B3LYP	RI-CC2	RI-CC2[b]
TrBD	5.63	5.74	5.89	6.15	6.13[c]
	(0.64)	(0.66)	(0.69)	(0.74)	(0.73)
CBD	5.04	5.13	5.25	5.48	
	(0.30)	(0.30)	(0.30)	(0.30)	
ACR	3.42	3.49	3.65	3.55	
	(0.00)	(0.00)	(0.00)	(0.00)	
ACT	4.41	4.46	4.50	4.49	4.45[c]
	(0.00)	(0.00)	(0.00)	(0.00)	(0.00)
PYR	6.08	6.25	6.28	6.28	6.42[c]
	(0.18)	(0.19)	(0.18)	(0.17)	(0.001)
DZM	2.99	3.05	3.01	3.30	
	(0.00)	(0.00)	(0.00)	(0.00)	
PAA	3.64	3.85	4.31	3.86	
	(0.00)	(0.00)	(0.00)	(0.00)	
MDB	4.21	4.29	4.38	4.24	4.20[d]
	(0.63)	(0.64)	(0.68)	(0.74)	n/a
MDC	3.47	3.54	3.60	3.36	3.33[d]
	(1.00)	(1.02)	(1.08)	(1.18)	n/a
MDD	3.01	3.06	3.13	2.85	2.82[d]
	(1.34)	(1.37)	(1.42)	(1.56)	n/a
JM	3.24	3.32	3.53	3.13	
	(0.77)	(0.80)	(0.84)	(0.86)	
IDMN	3.36	3.44	3.63	3.33	
	(0.89)	(0.93)	(1.00)	(1.07)	
FR0	3.25	3.40	3.87	3.58	
	(0.67)	(0.72)	(0.85)	(0.90)	
PRODAN	3.43	3.56	3.93	3.58	
	(0.30)	(0.30)	(0.27)	(0.29)	
4-AP	3.63	3.78	4.09	4.00	
	(0.07)	(0.07)	(0.08)	(0.07)	

[a]Oscillator strength are given in the row below in parentheses. [b]RI-CC2 data taken from literature. [c]Ref 8. [d]Ref 50.

Concerning the expected accuracy, Schreiber et al.[8,29] outlined in a comprehensive benchmark series containing a set of chemically similar molecules that CC2 in combination with a triple-ζ basis set yields on average transition energies that are higher than those for CC3/CASPT2 by a mean deviation of +0.10−0.20 eV whereas it surpasses results obtained from a CCSD model. In this context, we note that their vertical RI-CC2/aVTZ absorption energies for TrBD (6.13 eV), ACT (4.65 eV), and PYR (6.42 eV) computed at MP2-optimized ground-state structures agree very well with our transition energies of 6.15 eV, 4.49 eV, and 6.28 eV, respectively, calculated at the corresponding RI-CC2 ground-state structures. These findings seem to eliminate any sizable geometrical effects on the vertical excitation energies in question for at least the latter π-systems.

In light of the above trends, we conclude that in the present case the PBE0 hybrid functional provides the best compromise with respect to RI-CC2 for the considered $n \rightarrow \pi^*$ and $\pi \rightarrow \pi^*$ excitations in our selection of small and extended organic chromophores. We also note, however, that the mean absolute errors (MAE) of all the three functionals are very close (0.22, 0.15, and 0.23 eV for B3LYP, PBE0, and CAM-B3LYP, respectively). Moreover, values of standard deviation (SD) and relative standard deviation (RSD) per functional show that the dispersion is larger for B3LYP (RSD = 70%) and PBE0 (RSD = 80%) than for CAM-B3LYP (RSD = 59%). We can therefore

conclude that MAEs are not really different, and for all functionals MAE is around 0.2 eV. The performances are thus in line with our precedent work[18] and with benchmark studies of Jacquemin et al.[45] for singlet valence excitations. Moreover, in analyzing the excitations by means of the Λ diagnostic,[5] no marked CT character was found for the excitations studied: Λ > 0.4 for all systems with the exception of PAA (see Table 2).

Table 2. Λ Diagnostic Parameter Computed at the DFT/6-311++G(d,p) Level of Theory for All the Investigated Systems in Their Ground State Geometries

system	B3LYP	PBE0	CAM-B3LYP
TrBD	0.86	0.86	0.85
CBD	0.86	0.86	0.83
ACR	0.47	0.47	0.46
ACT	0.52	0.51	0.43
PYR	0.74	0.74	0.67
DZM	0.45	0.46	0.45
PAA	0.29	0.29	0.26
MDB	0.74	0.74	0.72
MDC	0.72	0.72	0.69
MDD	0.72	0.72	0.68
JM	0.67	0.67	0.65
IDMN	0.73	0.73	0.71
FR0	0.58	0.59	0.58
PRODAN	0.68	0.69	0.66
4-AP	0.63	0.63	0.63

3.1.2. Excited State Structures and Emission Energies. As for the ground-state, also for the singlet excited-state equilibrium geometrical parameters we refer to RI-CC2 geometries (see Figure 5 for small molecules and Figure 6 for extended systems).

In the comparison of TD-DFT and RI-CC2 results for the small molecules, it is important to preliminarily note that the RI-CC2 optimized excited state structures do not follow any obvious pattern when compared to the CASPT2 data of Page and Olivucci.[50] The RI-CC2/CASPT2 agreement ranges from good (CBD and TrBD) with shorter C−C single and double bonds of up to 0.01 Å, to satisfactory (PYR) to notably poor (ACR, ACT, and PAA). The high values of the D_1 (0.12−0.13) and D_2 (0.21−0.22) diagnostics (see Table 3) together with the low percentage of single-excitation character lead us to the conclusion that we encounter a (near) breakdown of the CC2 model for the particular cases of the excited-state carbonyl- and carboxylate compounds ACR, ACT, and PAA.

Given in addition the fact that the CC2 approach is known to yield too long carbon−oxygen bonds in carbonyl compounds after $n \rightarrow \pi^*$ excitations,[41] we consider our RI-CC2 geometrical data including the vertical emission energies at least questionable for these three compounds. As a matter of fact, ACR and ACT are the systems for which we observe the largest differences between RI-CC2 and the various TD-DFT results.

A similar conclusion can be drawn for the heteroaromatic bis-annular system 4-AP. We first note that the BLA parameter for the excited state calculated at the RI-CC2 level varies significantly from the remaining values calculated by means of TD-DFT. Second, whereas TD-DFT/PBE0 and TD-DFT/B3LYP predict a neutral form of 4-AP in the $\pi-\pi^*$ excited state (BLA > 0), CAM-B3LYP and RI-CC2 yield a (slightly) charge-separated zwitterionic state. The sizable discrepancy between CAM-B3LYP, which by construction should perform well in such a case, and RI-CC2 may thus be explained by the significant multireference character of the underlying ground-state CC2 wave function which is indicated by D_1 and D_2 values of 0.14 and 0.22, respectively. Furthermore, the considered state exhibits a notable percentage of double excitation character as revealed by the low single excitation biorthogonal norm $\%\langle \bar{E}_1 | E_1 \rangle$ of 85% computed from the CC2 response equations. Taken together, the validity of the CC2 *ansatz* may strongly be doubted for 4-AP at the excited state geometry.

Considering the remaining conjugated systems we observe BLA parameter curves from TD-DFT/CAM-B3LYP and RI-

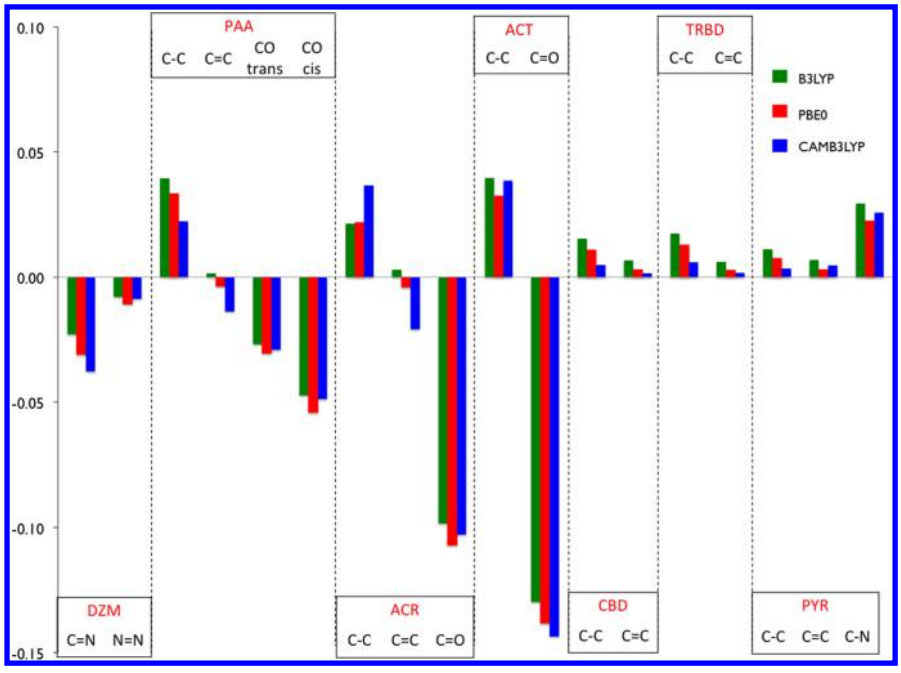

Figure 5. Differences in bond lengths (in Å) of excited state geometries calculated at the DFT/x level with respect to RI-CC2 values.

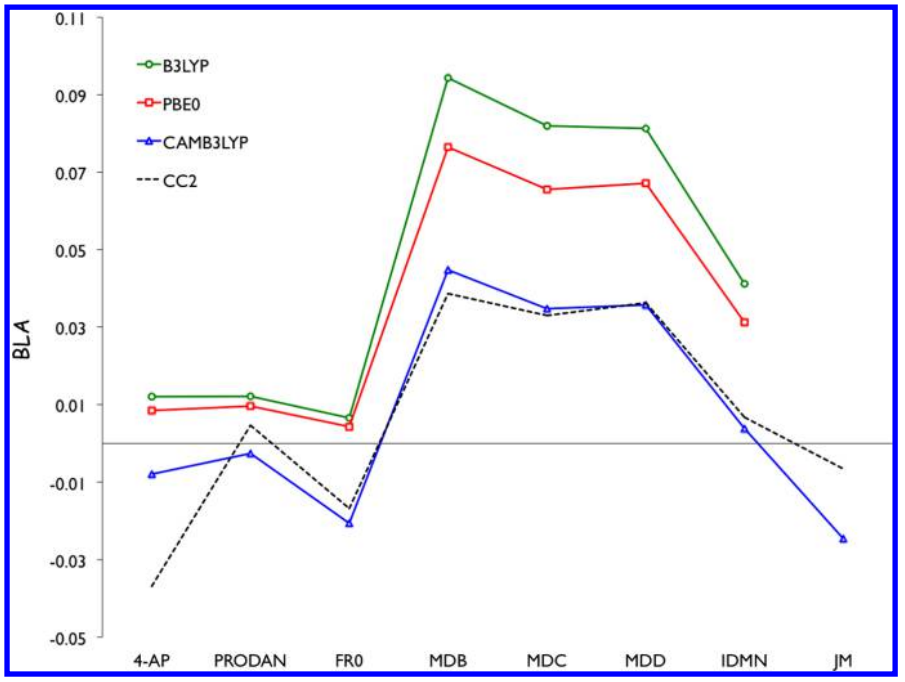

Figure 6. Excited state bond-length alternation (BLA) computed at the DFT/x and RI-CC2 level of theory.

Table 3. Measures of the Quality of the RI-CC2 Wave Function Obtained with the aVTZ Basis Set at the Optimized Excited State Structures of Selected Molecules[a]

molecule	state	D_1	D_2	$\%\langle\bar{E}_1\|E_1\rangle$
ACR	$n \rightarrow \pi^*$	0.1293	0.2135	87.91
ACT	$n \rightarrow \pi^*$	0.1299	0.2112	89.04
PAA	$n \rightarrow \pi^*$	0.1207	0.2154	85.25
4-AP	$\pi \rightarrow \pi^*$	0.1430	0.2236	84.91

[a]The D_1 and D_2 measures assess the quality of the ground-state wave function. The biorthogonal norm $\%\langle\bar{E}_1|E_1\rangle$ gives the percentage of single-excitation contribution to the excitation.

CC2 in close agreement following each other almost in parallel where the largest deviation of −0.18 Å emerges for JM. The expected chemical picture of a charge-separated state in this strong push−pull system is predicted correctly in either case, though. Valsson and Filippi[52] optimized the MDx systems at the CASPT2 and CC2 levels of theory using a small double-ζ basis set. They observed the largest deviations between their CASPT2 (0.025 Å) and CC2 (0.040 Å) single- and double bond length variations for the smallest system MDB. This trend is confirmed by our present RI-CC2/aVTZ data with a BLA of 0.039 Å for the optimized excited state geometry. Interestingly, the BLA for MDB is close in magnitude with respect to the extended model systems MDC (0.033 Å) and MDD (0.036 Å) which emphasizes the persistent localized character of single- and double bonds in the excited state in either system. In this context, TD-DFT/PBE0 and TD-DFT/B3LYP exaggerate this picture, although the relative trend with the addition of two vinyl groups from MDC to MDD is reproduced correctly.

Moving to vertical emission energies (see Table 4), the performance and reliabilty of RI-CC2 as a reference for TD-DFT is less unambiguous than it was the case for the vertical singlet absorption energies in the previous paragraph.

As shown in Table 4 the overall trend resulting from TD-DFT in combination with the three xc functionals clearly marks a few outliers in RI-CC2 for the carbonyl and carboxylic acid

Table 4. Computed Vertical Emission Energies (eV) at the DFT/6-311++G(d,p) and RI-CC2/aVTZ Level of Theory[a]

system	B3LYP	PBE0	CAM-B3LYP	RI-CC2
TrBD	4.93	5.02	5.03	5.49
	(0.66)	(0.68)	(0.69)	(0.76)
CBD	4.08	4.15	4.14	4.54
	(0.23)	(0.23)	(0.22)	(0.22)
ACR	2.70	2.80	3.08	2.29
	(0.00)	(0.00)	(0.00)	(0.00)
ACT	3.07	3.14	3.20	2.41
	(0.00)	(0.00)	(0.00)	(0.00)
PYR	5.52	5.66	5.61	5.84
	(0.20)	(0.21)	(0.21)	(0.19)
DZM	2.57	2.61	2.52	2.95
	(0.00)	(0.00)	(0.00)	(0.00)
PAA	1.48	1.59	2.07	0.83
	(0.00)	(0.00)	(0.00)	(0.00)
MDB	3.91	4.02	4.07	3.88
	(0.53)	(0.58)	(0.68)	(0.71)
MDC	3.26	3.37	3.44	3.17
	(0.81)	(0.91)	(1.09)	(1.15)
MDD	2.78	2.89	2.99	2.69
	(0.98)	(1.13)	(1.42)	(1.45)
JM	1.53	1.70	3.25	2.92
	(0.00)	(0.00)	(0.81)	(0.81)
IDMN	2.88	3.05	3.33	2.94
	(0.62)	(0.73)	(0.95)	(0.93)
FR0	3.10	3.26	3.49	3.27
	(0.70)	(0.77)	(0.96)	(1.00)
PRODAN	3.12	3.24	3.51	3.22
	(0.24)	(0.24)	(0.28)	(0.26)
4-AP	3.07	3.19	3.42	2.70
	(0.05)	(0.05)	(0.06)	(0.00)

[a]Oscillator strength are given in the row below in parentheses.

compounds ACR, ACT, PAA ($\pi \rightarrow n^*$), and 4-AP ($\pi^* \rightarrow \pi$) with deviations >1.0 eV thus calling for further attention. As

dx.doi.org/10.1021/ct400021c | J. Chem. Theory Comput. 2013, 9, 2209−2220

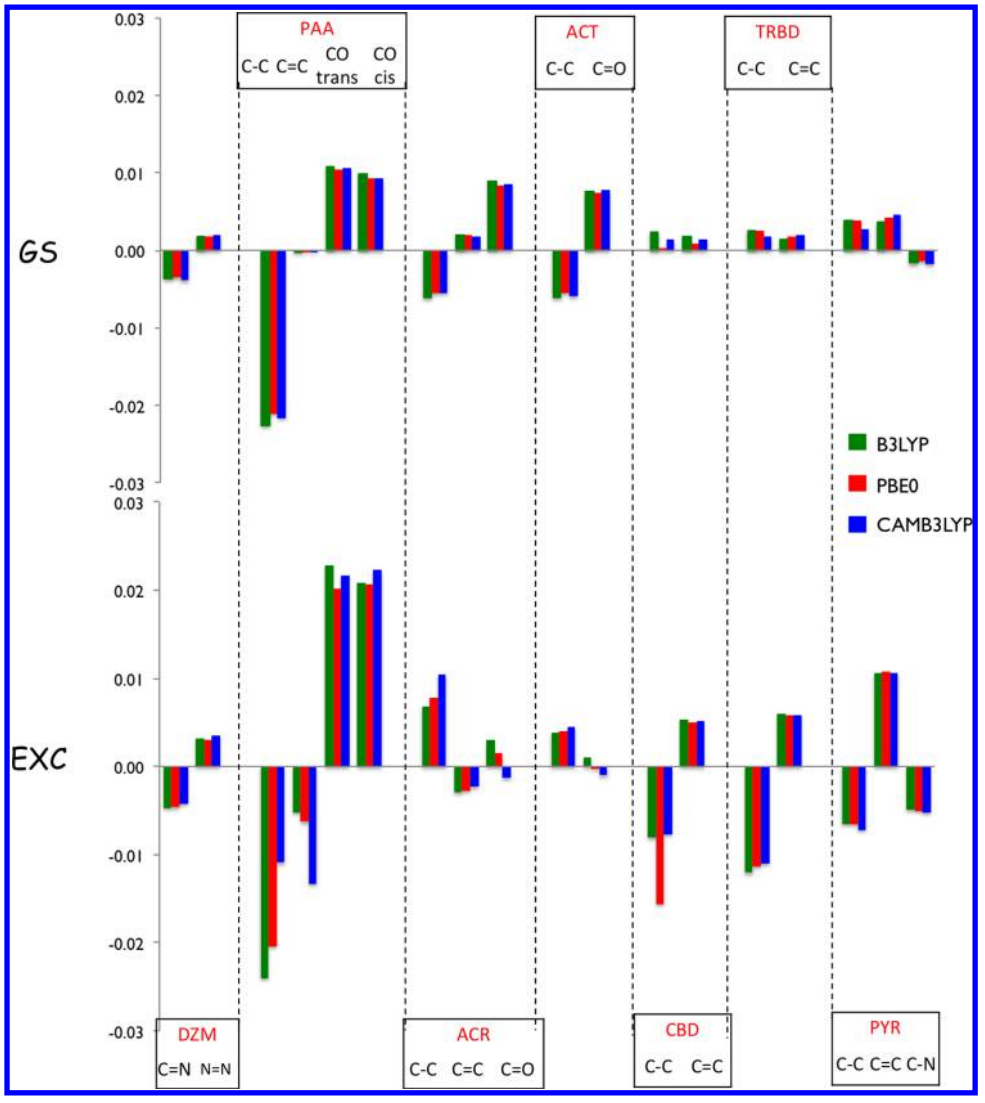

Figure 7. Differences in bond lengths (Å) for the solvated molecules (in ACN) with respect to gas-phase geometries. The upper plot refers to ground state geometries and the lower plot to excited state geometries.

aforementioned, it is easily seen from Table 3 that the known limits for the CC2 model (D_1: 0.10−0.15; D_2: 0.20−0.25) are distinctly approached in all four cases not only for D_1 and D_2, respectively, but more importantly also a significant amount of double excitation character enters the respective excited state wave function where $\%\langle \bar{E}_1 | E_1 \rangle \leq 89\%$. With unreliable excited-state geometries at hand (*vide supra*) because of a breakdown of the CC2 model, the exceedingly large deviations in emission energies may therefore not be unexpected. TD-DFT on the contrary seems to provide for these four molecules more stable results as variations among the three xc-functionals are 0.5 eV or less where the excited state emission is most sensitive to the amount of exact exchange only for the anion PAA. For JM, all our attempts to obtain a "regular" $\pi \rightarrow \pi^*$ excited structure for B3LYP and PBE0 failed because the optimization led in either case to a twisted structure where the excited state evidently has a different character as indicated by the low oscillator strength.

In principle, even if the Kohn−Sham (KS) implementation of DFT is single reference, if we knew the exact XC functional we could also include both static and dynamic correlation. The ability of TD-DFT to partly describe the charge-transfer/double-excitation character may actually be a result of a fortuitous cancellation of errors due to the use of approximate XC functionals which may give rise to unphysical fractional charges and fractional spins.[53] It is known that LDA and moreover GGA exchange include some static and dynamic correlation. This was first recognized by Cohen and Handy[54,55] and by the extended studies of Cremer and co-workers.[56,57] This may explain why, for example, GGA and in some cases also LDA outperform HF. For some diatomics, Cremer and co-workers analyzed the density differences with respect to MP2, MP3, MP4, CCSD, and CCSD(T) showing that the obtained density is usually more similar to more correlated methods than to pure HF. A rigorous way of introducing static and dynamic correlation by virtue of range separation into a hybrid KS-DFT-multireference wave function framework has recently been presented by one of the authors (S.K.).[58] This approach will be suitable for chromophores with large double-excitation characters and/or (long-range) charge-transfer excitations in their lowest singlet excited states.

With the 10 molecules remaining we note that the trends, established in the preceding paragraph for the absorption process, last to a considerable extent also for the emission energies. While B3LYP with the lowest amount of exact

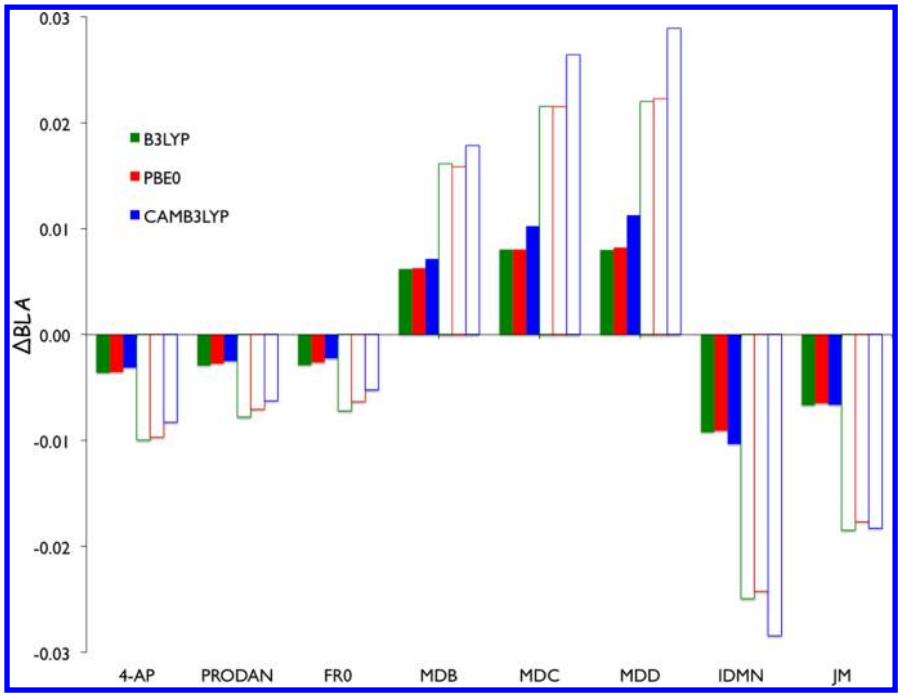

Figure 8. Differences in the BLA parameter (in Å) for the solvated GS structures with respect to gas-phase. Full histograms refer to cyclohexane while empty ones to acetonitrile.

exchange consistently yields the lowest emission energies among the three functionals, with the exception of DZM, PBE0 and CAM-B3LYP generally close ranks for the de-excitation energies in comparison to the absorption spectra. In summary, PBE0 nevertheless still gives the best overall agreement with RI-CC2 exhibiting a maximum deviation of 0.47 eV in TrBD whereas oscillator strength are in general better reproduced with CAM-B3LYP.

Based on the above geometrical analysis it seems clear that no single xc-functional can be chosen for the best performance of both ground and excited state geometries. For the ground state structures PBE0 and B3LYP perform almost identical and better than CAM-B3LYP compared to RI-CC2 predictions. For the excited state geometries PBE0 and CAM-B3LYP exhibit a slightly better performance for the smaller systems than B3LYP. However, for the larger conjugated systems CAM-B3LYP is clearly the most suitable choice.

3.2. Solvated Systems. To quantify the effects of the environment, we compare the solvent-induced shifts on geometries analyzing the small and the larger conjugated molecules, separately.

3.2.1. Small Molecules. In Figure 7 differences in bond lengths with respect to gas-phase geometries are shown for the ground and the excited states of the small solvated molecules in acetonitrile. The parallel shifts for cyclohexane are not shown as they are very similar to those obtained in acetonitrile but only smaller in magnitude.

The effect of introducing the PCM environment in the calculation of the geometries is quite limited for all the investigated small molecules: the bond length changes are around or less than 0.01 Å, that is, smaller than the average difference between DFT and RI-CC2, with the only exception of C−C in PAA for which we observe a shortening of about 0.02 Å. In addition, the three investigated functionals give very similar descriptions.

Moving to excited state structures, we have to stress that for these systems the electron density reorganization remains relatively small, therefore we do not expect large solvent effects. The lower plot in Figure 7 shows that this is indeed the case, and in fact all shifts are less than 0.03 Å . Moreover, as already observed for the ground states, the differences among functionals are very small.

Comparing Figure 5 and Figure 7, we can conclude that also in solvated systems, for $\pi \rightarrow \pi^*$ excitations both global and range-separated functionals perform very well in describing structures of small systems. For $n \rightarrow \pi^*$ excitations, that involve a more pronounced variation of the density, the solvent effect is slightly larger than in the $\pi \rightarrow \pi^*$ case, and a better description is obtained by means of CAM-B3LYP. This is also in line with the analysis of vertical excitation energies as a function of the Λ diagnostic (see Table 2) usually $\Lambda(n \rightarrow \pi^*) < \Lambda(\pi \rightarrow \pi^*)$.[5,12]

3.2.2. Conjugated Molecules. To verify whether the conclusions drawn for the small systems also hold for the larger conjugated systems, we analyze the solvent induced changes in the structures in terms of the collective geometrical BLA parameter. In Figure 8 the change in the ground state BLAs moving from gas-phase to solution is depicted for the two different solvents and the three functionals.

As it can be seen from Figure 8, both solvents reduce the BLAs of all the neutral systems (4-AP, PRODAN, FR0, IDMN, and JM). This clearly illustrates that all the functionals here investigated equally describe the solvent effect as an increase of the charge-transfer character of the GS of these conjugated systems. This is indeed what we would expect on the basis of a valence-bond picture in which an increase of the polarity of the solvent corresponds to a larger contribution of the zwitterionic-like form.

On the contrary, the protonated MDx (x = B,C,D) systems show an increased BLA in both solvents for all the functionals, with CAM-B3LYP showing the largest shifts. Once more, these findings can be explained in terms of the valence-bond picture:

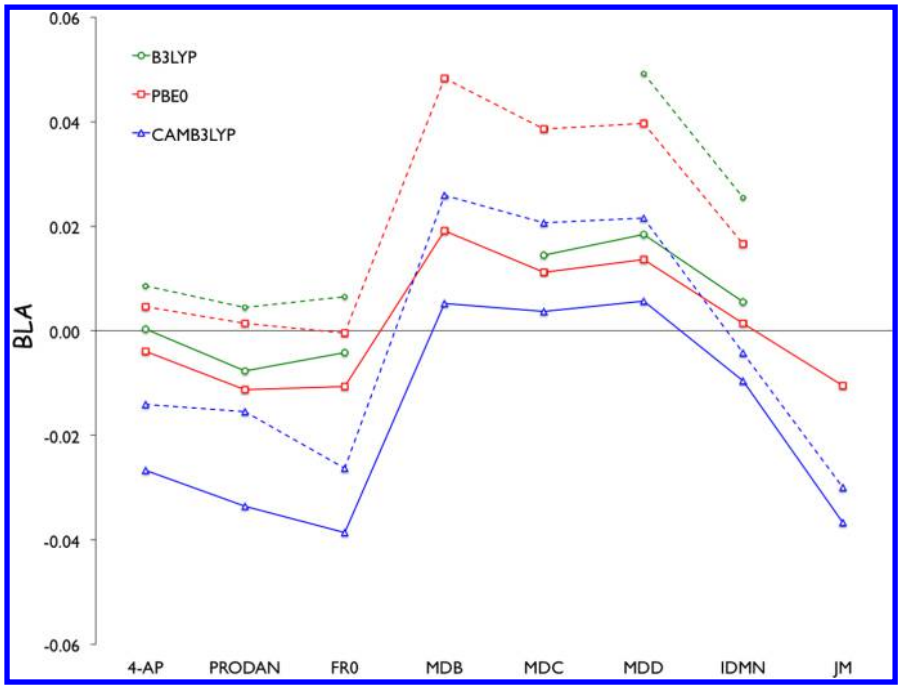

Figure 9. Excited state BLAs (in Å) for the larger conjugated systems in solution. Dotted lines refer to cyclohexane while full ones to acetonitrile.

for the MDx systems in fact the so-called "neutral" form is the one in which the charge is more localized and therefore we expect that the presence of the solvent will amplify its contribution.

In conclusion, for the GS structures the solvent effect is almost independent of the functional for the neutral compounds, whereas a larger effect is found increasing the HF exchange for charged systems. Once again, we can therefore conclude that the results found in gas-phase, namely, that the best performances with respect to RI-CC2 are obtained by using PBE0 (and almost equivalently B3LYP), are still valid also in the case of solvated systems.

Moving to excited states, we thus would expect that solvent effects lead to smaller BLAs for all neutral and charged molecules, and this is indeed what we observe with all three functionals. In this case, to facilitate a more quantitative analysis of the differences among the functionals, it is more useful to compare the real value of the BLAs rather than their shift with respect to gas-phase. These data are reported in Figure 9.

As illustrated in Figure 9 the differences among the different functionals are much larger than in the ground state case. In particular, only CAM-B3LYP leads to negative BLAs for all the neutral systems (4-AP, PRODAN, FR0, IDMN, and JM) in both solvents. Both B3LYP and PBE0 in fact present BLAs very close to zero or even positive in the apolar solvent. We recall that a more negative value of the BLA means that the system is better described as a zwitterion which is exactly what is expected for the excited states of push−pull systems when increasing the polarity of the environment. We also emphasize that only CAM-B3LYP manages to optimize a planar excited state structure for all systems while the other two functionals fail for JM and for some of the PBS systems (especially B3LYP in the apolar solvent).

3.2.3. Emission Energies. To conclude the analysis on solvent effects we report in Table 5 the shifts in the emission energies of all the investigated systems moving from gas-phase to acetonitrile. In particular, two sets of data are reported for each functional, namely, the shifts obtained by keeping the gas-phase structure of each excited state and the parallel shifts obtained using the solvated structures. In this analysis, only the polar solvent has been considered in combination with the PBE0 or the CAM-B3LYP functionals since B3LYP has in fact shown large limitations in the correct determination of the excited state structures to be properly used for the evaluation of emission energies in gas-phase and the corresponding solvatochromic shifts.

Table 5. Gas-to-Acetonitrile Shifts in the Emission Energies (in eV) for All the Investigated Systems Obtained Using Either the Gas-Phase (geom@gas) or the Solvated (geom@ACN) Geometries

	PBE0		CAM-B3LYP	
System	geom@gas	geom@ACN	geom@gas	geom@ACN
TrBD	−0.03	−0.09	−0.03	−0.10
CBD	−0.03	−0.11	−0.03	−0.05
ACR	−0.03	0.00	0.00	0.04
ACT	0.06	0.05	0.06	0.06
PYR	−0.06	−0.11	−0.04	−0.10
DZM	−0.11	−0.12	−0.12	−0.13
PAA	0.45	0.29	0.51	0.39
MDB	0.03	0.04	0.03	−0.03
MDC	0.04	−0.15	0.03	−0.26
MDD	0.02	0.04	0.02	−0.12
JM			−0.20	−0.19
IDMN	−0.26	−0.09	−0.13	−0.12
FR0	−0.71	−0.69	−0.44	−0.54
PRODAN	−0.43	−0.41	−0.31	−0.35
4-AP	−0.72	−0.74	−0.66	−0.71

In this analysis the differences between the two functionals are more evident. In particular only CAM-B3LYP seems to display a rational behavior with respect to the characteristics of the systems (neutral vs charged, small vs largely conjugated) and of the excitations ($\pi-\pi^*$ vs $n-\pi^*$). For most of the small

neutral systems, the solvatochromic shift obtained using the gas-phase structures is significantly underestimated (TrBD,CBD,ACR,PYR) whereas for the large conjugated systems the gas-phase and the solvated geometries give more similar shifts (JM, IDMN, FR0, PRODAN, 4-AP). This behavior is apparently in contrast with what is observed for the geometries: in the push−pull systems the solvent effects on the excited state BLAs were quite large. Therefore, the reason why the solvatochromic shifts are reasonably similar with the two geometries is that both the excited state and the vertical ground state energies are similarly affected by the change in the geometry. This is not unexpected as push−pull systems are easily polarizable by a solvent even in their ground state. In the case of charged systems instead quite different behaviors are found: For PAA the relaxation of the geometry partially cancels the large blue-shift found with the gas-phase geometry while for the MDx series it leads to a change in the sign of the shift reverting to red-shifts as expected from the $\pi-\pi^*$ character of the excitation.

If we collectively compare all these results with those obtained for the gas phase (Figure 6), we can conclude that the most correct description of solvent effects is obtained with the CAM-B3LYP functional. This functional in fact, even if it generally overestimates vertical energies, gives a better description of the nature of the excited state, and, as a result, leads to better geometries and better solvatochromic effects. This crucial role of range-separated hybrid functionals was already noted by two of the present authors in simulating resonant Raman scattering of IDMN and JM[30] and the vibronic effects on emission spectrum of Nile Red.[59]

A final and definitive proof of these findings would be a comparison with experiments. Unfortunately this cannot be done for excited state geometrical parameters for which only indirect checks are possible. Among these, the solvatochromic shifts for emission energies are apparently the most straightforward. However, this analysis is less simple than it appears for different reasons. First of all in our study we have used a purely electrostatic solvation model: electrostatic effects are expected to be largely dominant in determining geometry relaxations, but they can be not sufficient to get accurate transition energies for which nonelectrostatic effects such as dispersion can play an important role.[60] In addition, experimental emission energies, when available, are generally obtained as the band maxima and therefore they are subject to vibronic and other broadening effects. A possible strategy to minimize the effects of these aspects that are not taken into account in our model is to focus on the shifts moving from an apolar to a polar solvents: if we thus assume that both nonelectrostatic and broadening effects are not largely solvent dependent, the measured shifts can be more fairly compared with the calculated ones. Indeed, for the few systems for which measured data are available (4-AP, PRODAN, FR0), CAM-B3LYP has shown to give solvatochromic shifts in very good (almost quantitative) agreement with experiments.[18]

4. SUMMARY

Nowadays TD-DFT represents the most popular approach for the calculation of transition energies, but its use is rapidly increasing also for the evaluation of excited state geometries and emission processes. While many studies have been performed on the potentials and limits of TD-DFT for vertical absorption energies, its performance in the characterization of electronic and geometrical relaxation following the ground-to-excited state transition is much less explored. In this study we have investigated the behavior of three of the most popular exchange-correlation functionals with respect to the characterization of the structures of a set of common organic chromophores in gas-phase *and* in solution. In particular, we have comparatively analyzed the combination of these functionals with one of the most widespread solvation models (PCM).

The overall results suggest that the long-range corrected exchange-correlation functional (CAM-B3LYP) captures the characteristics of the different excited states in a more rational way than the other two hybrid functionals. This superior behavior of CAM-B3LYP is first quantified by a numerical comparison to RI-CC2 results and further emphasized in terms of the behaviors one should expect on the basis of the nature of the excitation, the chemical bonds present in the investigated system, and the environment. Unfortunately, the same functional does not perform equally well for ground-state geometries and vertical absorption energies for which PBE0 and B3LYP clearly outperform CAM-B3LYP. Further analyses have therefore to be done as well as more extended sets of chromophores have to be investigated. However, the present study in line with those already present in the literature[14−18] seems to indicate that the absorption process and the following excited state relaxation presently cannot be described with sufficient accuracy by a single DFT functional.

AUTHOR INFORMATION

Corresponding Author

*E-mail: ciro.guido@ecp.fr (C.A.G.), knecht@sdu.dk (S.K.), kongsted@sdu.dk (J.K.), bene@dcci.unipi.it (B.M.).

Notes

The authors declare no competing financial interest.

ACKNOWLEDGMENTS

S.K. gratefully acknowledges a postdoctoral research grant from the Natural Science Foundation (FNU) of the Danish Agency for Science, Technology and Innovation (Grant 10-082944). J.K. thanks the Danish Center for Scientific Computing, The Danish Councils for Independent Research (STENO and Sapere Aude programmes), the Lundbeck Foundation, and the Villum foundation for financial support.

REFERENCES

(1) Runge, E.; Gross, E. K. U. *Phys. Rev. Lett.* **1984**, *52*, 997−1000.
(2) Casida, M. E. In *Time-Dependent Density-Functional Response Theory for Molecules*; Chong, D. P., Ed.; Recent Advances in Density Functional Methods; World Scientific: Singapore, 1995; Vol. *1*; pp 155−192.
(3) Dreuw, A.; Head-Gordon, M. *Chem. Rev.* **2005**, *105*, 4009−4037.
(4) Silva-Junior, M. R.; Schreiber, M.; Sauer, S. P. A.; Thiel, W. *J. Chem. Phys.* **2008**, *129*, 104103.
(5) Peach, M. J.; Benfield, P.; Helgaker, T.; Tozer, D. J. *J. Comput. Phys.* **2008**, *128*, 044118.
(6) Silva-Junior, M. R.; Schreiber, M.; Sauer, S. P. A.; Thiel, W. *J. Chem. Theory Comput.* **2009**, *5*, 555−564.
(7) Goerigk, L.; Moellmann, J.; Grimme, S. *Phys. Chem. Chem. Phys.* **2009**, *11*, 4611−4620.
(8) Silva-Junior, M. R.; Sauer, S. P. A.; Schreiber, M.; Thiel, W. *Mol. Phys.* **2010**, *108*, 453−465.
(9) Jacquemin, D.; Perpète, E. A.; Ciofini, I.; Adamo, C. *Theor. Chem. Acc.* **2011**, *128*, 127−136.
(10) Caricato, M.; Trucks, G. W.; Frisch, M. J.; Wiberg, K. B. *J. Chem. Theory. Comput.* **2011**, *7*, 456−166.

(11) Huix-Rotllant, M.; Ipatov, A.; Rubio, A.; Casida, M. E. *Chem. Phys.* **2011**, *391*, 120−129.
(12) Leang, S. S.; Zahariev, F.; Gordon, M. S. *J. Chem. Phys.* **2012**, *136*, 104101.
(13) Jacquemin, D.; Perpete, E. A.; Scuseria, G. E.; Ciofini, I.; Adamo, C. *J. Chem. Theory. Comput.* **2008**, *4*, 123−135.
(14) Le Bahers, T.; Pauporté, T.; Scalmani, G.; Adamo, C.; Ciofini, I. *Phys. Chem. Chem. Phys.* **2010**, *11*, 11276−11284.
(15) Guthmuller, J. *J. Chem. Theory. Comput.* **2011**, *7*, 1082−1089.
(16) Jacquemin, D.; Mennucci, B.; Adamo, C. *Phys. Chem. Chem. Phys.* **2011**, *13*, 16987−16998.
(17) Kupfer, S.; Guthmuller, J.; Gonzalez, L. *J. Chem. Theory. Comput.* **2013**, *9* (1), 543−554.
(18) Guido, C. A.; Jacquemin, D.; Adamo, C.; Mennucci, B. *J. Phys. Chem. A* **2010**, *114*, 13402−13410.
(19) Mennucci, B. *WIREs Comput. Mol. Sci.* **2012**, *2*, 386−404.
(20) DeFusco, A.; Minezawa, N.; Slipchenko, L. V.; Zahariev, F.; Gordon, M. S. *J. Phys. Chem. Lett.* **2011**, *2*, 2184−2192.
(21) Jacquemin, D.; Planchat, A.; Adamo, C.; Mennucci, B. *J. Chem. Theory. Comput.* **2012**, *8*, 2359−2372.
(22) Tomasi, J.; Mennucci, B.; Cammi, R. *Chem. Rev.* **2005**, *105*, 2999−3094.
(23) Adamo, C.; Barone, V. *J. Chem. Phys.* **1999**, *110*, 6158−6170.
(24) Ernzerhof, M.; Scuseria, G. E. *J. Chem. Phys.* **1999**, *110*, 5029−5036.
(25) Zhao, Y.; Truhlar, D. G. *Theor. Chem. Acc.* **2008**, *120*, 215−241.
(26) Yanai, T.; Tew, D. P.; Handy, N. C. *Chem. Phys. Lett.* **2004**, *393*, 51−57.
(27) Becke, A. D. *J. Chem. Phys.* **1993**, *98*, 5648−5652.
(28) Stephens, P. J.; Devlin, F. J.; Chabalowski, C. F.; Frisch, M. J. *J. Phys. Chem.* **1994**, *98*, 11623−11627.
(29) Schreiber, M.; Silva-Junior, M. R.; Sauer, S. P. A.; Thiel, W. *J. Chem. Phys.* **2008**, *128*, 134110.
(30) Mennucci, B.; Cappelli, C.; Guido, C. A.; Cammi, R.; Tomasi, J. *J. Phys. Chem. A* **2009**, *113*, 3009−3020.
(31) Marini, A.; Munoz-Losa, A.; Biancardi, A.; Mennucci, B. *J. Phys. Chem. B* **2010**, *114*, 17128−17135.
(32) Christiansen, O.; Koch, H.; Jörgensen, P. *Chem. Phys. Lett.* **1995**, *243*, 409−418.
(33) Hättig, C.; Weigend, F. *J. Chem. Phys.* **2000**, *113*, 5154.
(34) Cancès, E.; Mennucci, B.; Tomasi, J. *J. Chem. Phys.* **1997**, *107*, 3032−3041.
(35) Hättig, C.; Köhn, A. *J. Chem. Phys.* **2002**, *117*, 6939−6951.
(36) Hättig, C. *J. Chem. Phys.* **2003**, *118*, 7751−7761.
(37) Ahlrichs, R.; Bär, M.; Häser, M.; Horn, H.; Kölmel, C. *Chem. Phys. Lett.* **1989**, *162*, 165−169.
(38) Dunning, T. H., Jr. *J. Chem. Phys.* **1989**, *90*, 1007.
(39) Kendall, R. A.; Dunning, T. H., Jr.; Harrison, R. J. *J. Chem. Phys.* **1992**, *96*, 6769.
(40) Weigend, F.; Köhn, A.; Hättig, C. *J. Chem. Phys.* **2002**, *116*, 3175−3183.
(41) Köhn, A.; Hättig, C. *J. Chem. Phys.* **2003**, *119*, 5021−5036.
(42) Janssen, C. L.; Nielsen, I. M. B. *Chem. Phys. Lett.* **1998**, *290*, 423−430.
(43) Nielsen, I. M. B.; Janssen, C. L. *Chem. Phys. Lett.* **1999**, *310*, 568−576.
(44) Frisch, M. J.; Trucks, G. W.; Schlegel, H. B.; Scuseria, G. E.; Robb, M. A.; Cheeseman, J. R.; Scalmani, G.; Barone, V.; Mennucci, B.; Petersson, G. A.; Nakatsuji, H.; Caricato, M.; Li, X.; Hratchian, H. P.; Izmaylov, A. F.; Bloino, J.; Zheng, G.; Sonnenberg, J. L.; Hada, M.; Ehara, M.; Toyota, K.; Fukuda, R.; Hasegawa, J.; Ishida, M.; Nakajima, T.; Honda, Y.; Kitao, O.; Nakai, H.; Vreven, T.; Montgomery, Jr., J. A.; Peralta, J. E.; Ogliaro, F.; Bearpark, M.; Heyd, J. J.; Brothers, E.; Kudin, K. N.; Staroverov, V. N.; Kobayashi, R.; Normand, J.; Raghavachari, K.; Rendell, A.; Burant, J. C.; Iyengar, S. S.; Tomasi, J.; Cossi, M.; Rega, N.; Millam, J. M.; Klene, M.; Knox, J. E.; Cross, J. B.; Bakken, V.; Adamo, C.; Jaramillo, J.; Gomperts, R.; Stratmann, R. E.; Yazyev, O.; Austin, A. J.; Cammi, R.; Pomelli, C.; Ochterski, J. W.; Martin, R. L.; Morokuma, K.; Zakrzewski, V. G.; Voth, G. A.; Salvador, P.; Dannenberg, J. J.; Dapprich, S.; Daniels, A. D.; Farkas, O.; Foresman, J. B.; Ortiz, J. V.; Cioslowski, J.; Fox, D. J. *Gaussian 09*, Revision A.1; Gaussian Inc.: Wallingford, CT, 2009.
(45) Jacquemin, D.; Wathelet, V.; Perpéte, E. A.; Adamo, C. *J. Chem. Theory. Comput.* **2009**, *5*, 2420−2435.
(46) Jacquemin, D.; Perpéte, E. A.; Ciofini, I.; Adamo, C. *Acc. Chem. Res.* **2009**, *42*, 326−334.
(47) Jacquemin, D.; Adamo, C. *Int. J. Quantum Chem.* **2012**, *112*, 2135−2141.
(48) Caricato, M.; Mennucci, B.; Tomasi, J.; Ingrosso, F.; Cammi, R.; Corni, S.; Scalmani, G. *J. Chem. Phys.* **2006**, *124*, 124520.
(49) Marder, S. R.; Perry, J. W.; Bourhill, G.; Gorman, C. B.; Tiemann, B. G.; Mansour, K. *Science* **1993**, *261*, 186.
(50) Page, C. S.; Olivucci, M. *J. Comput. Chem.* **2003**, *24*, 298−309.
(51) Helgaker, T.; Ruden, T. A.; Jørgensen, P.; Olsen, J.; Klopper, W. *J. Phys. Org. Chem.* **2004**, *17*, 913−933.
(52) Valsson, O.; Filippi, C. *J. Chem. Theory. Comput.* **2010**, *6*, 1275−1292.
(53) Cohen, A. J.; Mori-Sánchez, P.; Yang, W. *Science* **2008**, *321*, 792−794.
(54) Handy, N. C.; Cohen, A. J. *Mol. Phys.* **2001**, *99*, 403−412.
(55) Cohen, A. J.; Handy, N. C. *Mol. Phys.* **2001**, *99*, 607−615.
(56) Cremer, D. *Mol. Phys.* **2001**, *99*, 1899−1940.
(57) Cremer, D.; Filatov, M.; Polo, V.; Kraka, E.; Shaik, S. *Int. J. Mol. Sci.* **2002**, *3*, 604−638.
(58) Fromager, E.; Knecht, S.; Jensen, H. J. A. *J. Chem. Phys.* **2013**, *138*, 084101.
(59) Guido, C. A.; Mennucci, B.; Jacquemin, D.; Adamo, C. *Phys. Chem. Chem. Phys.* **2010**, *12*, 8016−8023.
(60) Weijo, V.; Mennucci, B.; Frediani, L. *J. Chem. Theory. Comput.* **2010**, *6*, 3358−3364.